Published in J. Appl. Phys. 103, 073704 (2008).

Band Offsets of InGaP/GaAs Heterojunctions by Scanning Tunneling Spectroscopy

Y. Dong and R. M. Feenstra
Department of Physics, Carnegie Mellon University, Pittsburgh, Pennsylvania 15213

M. P. Semtsiv and W. T. Masselink
Department of Physics, Humboldt-Universität zu Berlin, D-10115 Berlin, Germany

Abstract

Scanning tunneling microscopy and spectroscopy are used to study InGaP/GaAs heterojunctions with InGaAs-like interfaces. Band offsets are probed using conductance spectra, with tip-induced band bending accounted for using 3-dimensional electrostatic potential simulations together with a planar computation of the tunnel current. Curve fitting of theory to experiment is performed. Using an InGaP band gap of 1.90 eV, appropriate to the disordered InGaP alloy, a valence band offset of 0.38 ± 0.01 eV is deduced along with the corresponding conduction band offset of 0.10 ± 0.01 eV (type I band alignment).

I. INTRODUCTION

Heterojunction band offset engineering has been extensively utilized over the past decade both for improved device design and to enable better understanding of the fundamental properties of interfaces.[1] It is important to relate the fundamental properties, *e.g.* band offsets, with the detailed microscopic nature of the interface. Scanning tunneling microscopy (STM) and spectroscopy (STS) are useful tools for this purpose.[2] It has been recently shown that possible complications in STS measurements due to tip-induced band bending can be effectively addressed using 3-dimensional electrostatic simulations along with a detailed computation of the tunneling current, thus enabling a quantitative interpretation of the experimental spectroscopic results.[3,4,5,6]

$In_xGa_{1-x}P$ with $x \approx 0.5$ (hereafter referred to as InGaP) is known to be lattice matched to GaAs. Its band gap is considerably larger than that of GaAs, so it has been proposed as an alternative to AlGaAs as a barrier material for heterostructures.[7] InGaP is potentially much better than AlGaAs for heterojunction bipolar transistors, since its much smaller conduction band (CB) offset results in a smaller electron-blocking spike that inhibits electron injection from the emitter into the base.[7] Depending on growth conditions, InGaP can exist either an *ordered* arrangement of cations or a *disordered* one, with band gaps of these forms differing by about 0.05 eV.[8] The InGaP studied in the present work is of the disordered variety,[9] with room-temperature band gap of about 1.90 eV.[10] The CB offset between InGaP and GaAs is known to be relatively small, [*i.e.* most of the band gap difference of $1.90 - 1.42 = 0.48$ eV is taken up in the valence band (VB)], although some disagreement exists in the literature as to its precise value.[9,10,11,12,13,14,15,16,17,18] Varying degrees of ordering in different samples could be one reason leading to these discrepancies of CB offset values,[19] with InGaP films grown by metal-organic chemical vapor deposition exhibiting more ordering than films grown by gas-source molecular beam epitaxy.[20,21] In addition, the heterointerface may also be InGaAs-like or GaP-like, thus providing another possible source of variation in band offset results.

In this work, cross-sectional STM and STS are used to study InGaP/GaAs heterojunctions grown by gas-source molecular beam epitaxy (GSMBE). Strain relaxation at the cleaved $(1\,\bar{1}\,0)$ face reveals the presence of InGaAs-like interfaces, consistent with the growth conditions employed. Band offsets of 0.10 ± 0.01 eV and 0.38 ± 0.01 eV (type I) for the CB and VB, respectively, are deduced on the basis of detailed curve fitting of the observed spectra with a theoretical model. This model consists of a 3-dimensional treatment of tip-induced band bending effects in the semiconductor, together with planar computation of tunnel current (using only the potential variation along the central axis of the problem) employing the Bardeen formalism. These band offset values are obtained assuming a value of 1.90 eV for the band gap of the InGaP layer, as appropriate for the disordered InGaP alloy layers that are observed in the STM images.[9] The result obtained here for the CB offset is somewhat larger than our earlier reported value of 0.04 ± 0.06 eV,[9] and we discuss in this work the inadequacy of the earlier analysis.

This paper is organized as follows. Experimental details are provided in Section II, with the data, both imaging and spectroscopic, presented in Section III. Our analysis is presented in Section IV where we make detailed fits of spectra acquired across a InGaP/GaAs heterojunction, using parameters of tip radius, tip-sample separation, tip-sample contact potential (work function difference), and the VB offset between tip and sample. Good fits are obtained between theory and experiment. In Section V we discuss the shortcomings of our previous analysis method.[9] Finally, in Section VI we summarize our results and we briefly discuss possible extensions to this work.

II. EXPERIMENTAL

A multilayer structure *p*-GaAs/*i*-InGaP/*p*-GaAs was grown on a *p*-type GaAs(001) substrate using gas-source molecular-beam epitaxy. The $In_xGa_{1-x}P$ was designed to be lattice matched with GaAs, with $x \approx 0.485$ (growth temperature is 430°C). GaAs layers are doped with Be at $1\times10^{18}\,\mathrm{cm}^{-3}$, while the 48-nm-thick InGaP is not intentionally doped. The growth procedure was designed to produce InGaAs-like interfaces, as discussed previously.[9] STM imaging clearly reveals the InGaP layer to be disordered.[9] An atomically flat $(1\,\bar{1}\,0)$ surface was formed by cleaving a sample in the scanning tunneling microscope (STM) chamber, under a background pressure of less than 5×10^{-11} Torr. Commercial Pt–Ir probe tips are used in STM/STS experiments. Topographic imaging is performed at a constant current of 0.1 nA and at sample voltages specified below.

Tunneling spectra were acquired at room temperature using a voltage modulation of 50 mV and employing a lock-in amplifier to obtain the differential conductance. The output time constant of the lock-in amplifier (10 ms) produces a slight voltage shift in our spectra, the magnitude of which is precisely known since we always acquire data in both the up-sweep and down-sweep directions. We perform a correction to our theoretically computed spectra, applying identically the same filter function to them as employed in the experiment. The technique of continuously varying tip-sample separation was used to obtain a large dynamic range in the measurements,[22] applying an offset to the tip-sample separation of the form $\Delta s(V) = a|V|$ where V is the voltage applied to the sample relative to the tip. Values of a are chosen to obtain conveniently measurable current and conductance values, with a value of about 0.1 nm/V typically being used (separate values of a are used for positive and negative voltages). For qualitative viewing of the spectra the measured values of conductance are then normalized by forming the ratio $(dI/dV)/(\overline{I/V})$, where some broadening is applied to (I/V) to produce a suitable normalization quantity;[5,22] we use a broadening of $\Delta V = 1.5\,\mathrm{V}$. For quantitative comparison of theory and experiment we use the conductance normalized to constant-s, formed by multiplying the measured conductance by $\exp(2\kappa\Delta s)$, where a constant value of $\kappa = 10\,\mathrm{nm}^{-1}$ is used. Importantly, in our computations we use identically the same Δs variation and normalization-to-constant-s procedure as in the experiment.

III. RESULTS
A. STM Imaging

Detailed STM images of our samples have been previously described,[9] and based on those results together with expectations from the growth conditions we concluded that the InGaP/GaP heterointerfaces were InGaAs-like (as opposed to GaP-like). That conclusion is further explored here by large-scale STM imaging of the morphology of the cleavage surface. Figure 1(A) shows an STM image of the heterostructure, with the InGaP layer appearing as the mottled region in the middle of the image. The (001) growth direction for the heterostructure, on this and all other STM images presented in this work, is towards the left. Single constant-current line scans acquired at various sample voltages are shown in Fig. 1(B), acquired from surface regions located within about 10 nm of the image of Fig. 1(A). A notable aspect of these data is that, as one moves into the GaAs layers from either side of the InGaP, the scans reveal a gradual downwards behavior in the surface morphology. This type of behavior is characteristic of a strained heterostructure,[23] revealing in this case a compressively-strained InGaP layer which protrudes slightly out of the cleavage surface.[24]

To demonstrate the consistency between the data of Fig. 1(B) and that expected for elastic relaxation of a strained heterostructure, we show by the dashed line in curve (d) of Fig. 1(B) the expected profiles for an InGaP layer that has uniform, in-plane (biaxial) compressive strain of 0.06% relative to the GaAs. This theoretical result is based on the elastic strain relaxation theory of Davies *et al*.[25] For comparison, the solid line in curve (d) [and also in curves (e) and (f)] shows the average of the experimental curves (a) – (c). We see that in the GaAs layers the computed profile agrees very well with the experiment, with the strain relaxation producing noticeable effects out to a distance of more than 100 nm from the heterointerfaces. However, within the InGaP layer itself the agreement between theory and experiment for curve (d) is rather poor. It is important to note that electronic effects will be relatively small at these voltages,[26] so that this disagreement implies some other type of strain in the heterostructure.

An alternative computation can be made by assuming that all of the strain arises from InGaAs-like interfaces, as expected from the growth conditions. The dashed line in curve (e) of Fig. 1(B) shows this result, where we have placed a single bilayer of InGaAs, with 3.36% biaxial strain relative to GaAs, at each heterointerface. In this case the agreement between experiment and theory within the InGaP and near the interfaces is quite good, but far into the GaAs the slope of the morphology is too small in the theory. A better match between experiment and theory is obtained by maintaining the InGaAs-like interfaces and adding a small amount of strain in the InGaP layer of 0.02%. The resulting theoretical curve is shown by the dashed line in curve (f) of Fig. 1(B).

B. Spatially-Resolved Spectroscopy

Detailed spectroscopic measurements have been performed near the heterointerfaces, with the goal of deducing band offsets. Results for an InGaP-on-GaAs interface are shown in Fig. 2. Eight white filled circles in the atomic-resolution image of Fig. 2(A)

shows the positions where the spectra in Fig. 2(B) were acquired. The location of the heterointerface is indicated by a dashed line in Fig. 2(A), located as the boundary between alloyed and nonalloyed regions as seen in STM images[9] (this boundary thus corresponds to the *metallurgical interface*, as discussed by Jäger *et al.*)[27]. Figure 2(A) as well as other STM images of the junctions also generally display a bright row of atoms right at the interface, consistent with the elastic strain relaxation of the InGaAs-like interfaces.[9]

In the spectra of Fig. 2(B) the approximate locations of the VB and CB edges are indicated using dashed lines. Examining the results, far into the InGaP layer we find a CB edge about 1.25 V while the VB edge is near -1.0 V. The difference between these results is 2.25 V, yielding an observed gap that is somewhat larger than known gap of 1.90 eV. At the GaAs layer, spectrum (a), the CB edge is again observed near 1.25 V and the VB edge at -0.55 V. The observed band gap thus has a width of about 1.7 eV, again somewhat larger than the known gap of 1.42 eV. We attribute these larger than expected observed gaps to tip-induced band bending in the semiconductor. Closely examining the spectra acquired between (a) and (h), we observe above the InGaP VB a tail of states originating from the GaAs VB. This result is expected, arising from the tails of the GaAs wavefunctions extending in the adjoining InGaP layer. For spectra (b) – (g) we thus see the VB state-density gradually evolving from that of GaAs to InGaP.

Following our previous work, we *qualitatively* estimate a band offset in Fig. 2, by overlaying at the bottom of the figure spectrum (a) from the GaAs layer on top of spectrum (h) from the InGaP layer. It appears that nearly all of the band gap difference between these materials is taken up in the valence band, with the difference in the CB edges between these spectra being only about 0.03 V. In the following sections we perform detailed fitting of the band onsets in order to more accurately determine this difference, and we find that the *qualitative* method just described actually produces a serious underestimate of the CB offset.

IV. ANALYSIS

A. Computation of Tunneling Spectra

To deduce values of the band offsets based on our spatially-resolved STS results, it is necessary to account for the effects of tip-induced band bending in the semiconductor. Our method for solving the 3-dimensional electrostatic problem has been previously described;[3] we use a finite-difference technique to obtain an exact solution for Poisson's equation in the vacuum and the semiconductor. For the present problem of a heterostructure an extension of the method is needed to describe the different materials, as detailed in the Appendix. An example of the theoretical results for the electrostatic potential is shown in Fig. 3 (we use the doping densities of the layers from Section II, and we assume a VB band offset of 0.36 eV between InGaP and GaAs although the results are very insensitive to this value since no charge transfer occurs between the layers). Importantly, our method for obtaining the potential distribution has been rigorously validated by taking the solution and using it as input to the *inverse* problem, as described in Ref. [4].

From our electrostatic computations we obtain the electrostatic potential energy at all points in the semiconductor and vacuum. We denote this quantity along the central axis of our problem as $\phi(z)$, and of particular interest is the potential energy at the point on the semiconductor surface directly opposite the tip apex, $\phi_0 \equiv \phi(0)$. This *surface band bending* is measured relative to the potential energy at a point far inside the semiconductor. With $\phi_0 \equiv 0$ we would have the usual relationship between energy of a state E and the sample voltage V, $E - E_F = eV$. With nonzero band bending this equation must be modified by shifting the energies by the surface band bending, as illustrated in Fig. 4(a), so that

$$E - E_F = eV - \phi_0 \quad . \tag{1}$$

This semiclassical formula assumes that the states shift rigidly in accordance with the band bending, *i.e.* as appropriate for *surface* states. But, for *bulk* states, additional quantum effect can occur as illustrated in Figs. 4(b) and (c). In particular, wavefunction tailing through a barrier region in the semiconductor, Fig. 4(b), can lead to substantial errors in the use of Eq. (1) to relate experiment and theory, particularly if the acquired spectra do not extend sufficiently far (>1 eV) from the band edge. For the present work such effects turn out to be relatively large, and an analysis based solely on Eq. (1) turns out to be inaccurate. In this case we must employ a complete computation of the conductance *vs.* voltage characteristics, comparing those results with experiment in order to deduce the values of parameters in the theory.

Band bending in the semiconductor depends on its intrinsic properties such as doping concentration and electron affinity, and additionally depends on three parameters of the tunnel junction: the tip-sample separation s, the tip radius-of-curvature R, and the work function of the metallic tip ϕ_m. To explain how the latter enters the computations we define a quantity $\Delta\phi$ as

$$\Delta\phi = \phi_m - \chi - \left(E_C - E_F\right) \tag{2}$$

where χ is the electron affinity of the semiconducting sample and $E_C - E_F$ is the difference between the CB minimum and the Fermi level deep inside the sample. The quantity $\Delta\phi$ defined in this way equals the *contact potential* between tip and sample in the absence of any extrinsic states on the sample surface.[28] Also, $eV + \Delta\phi$ is the difference between the electrostatic potential energies inside the tip compared to deep inside the semiconductor. In other words, with the zero in electrostatic potential energy taken to be deep inside the semiconductor, the electrostatic potential energy of the tip is given by $eV + \Delta\phi$. For GaAs its electron affinity is 4.13 eV,[29] and for 1×10^{18} cm^{-3} Be-doping $E_C - E_F = E_G - 78$ meV at 300 K with the gap being $E_G = 1.42$ eV. Therefore, values of $\Delta\phi$ and ϕ_m in this work are related by $\phi_m = 5.47\ \text{eV} + \Delta\phi$.

Defects and/or disorder on the cleaved surface may produce *extrinsic* states, which can act to produce surface charge and thereby affect the band bending in the semiconductor. As discussed in Ref. [4] such effects are small when the number of extrinsic states is less than about $0.01\,\mathrm{nm}^{-2}\mathrm{eV}^{-1}$, or about 0.003 monolayers spread over an energy range of 1 eV. For the present experiments the STM images generally indicate a lower number of residual defects than this (<0.002 monolayers as seen in large scale STM images), although we nevertheless include the possibility of extrinsic states in our analysis.

Using the full 3-dimensional solution for the electrostatic potential, we compute the tunnel current between tip and sample. We make one approximation for this purpose, assuming that the current can be obtained using only the potential along the central axis of our problem, $\phi(z)$, and then performing a *planar* tunneling computation with this potential. This approximation essentially amounts to a semiclassical treatment of the lateral (radial) part of the wavefunctions,[30] thus neglecting any quantization of the states arising from lateral variation of the potential. Those energy splittings have typical magnitude of 10 meV,[4,31] but any errors in band offsets due to this approximation should be much less than that since our work focuses on the *difference* in energies of states between GaAs and InGaP.

For a planar computation we have, in a series of prior papers,[3,4,5,6] developed a computation technique based on the Bardeen formalism[32] that permit computation of the tunnel current for a homogeneous semiconductor. For the present problem of a heterojunction between two different semiconductors a generalization of this method is required, as described in the Appendix. For the lateral (parallel) component of the wavefunction in the semiconductor we use, rather than simple plane waves, linear combination of incoming and outgoing states from the interface together with exponentially decaying evanescent states in the heterojunction barrier region. Combinations of such states are constructed to satisfy the boundary conditions for the wavefunctions at the heterointerface. In the computation of tunnel current we employ the Tersoff and Hamann approximation[33] by taking the tunnel current to be proportional to the local state-density at the apex of the probe tip.

Our computations include light, heavy, and split-off valence bands, together with a single conduction band. The results are not particularly sensitive to the effective masses, except for the light-hole mass of the VB which is quite important in determining the transmission of these states through the barrier region that occurs in the semiconductor. In this respect we use the VB mass in the [110] direction[34] in all our computations; this mass is fairly close to the spatially-averaged value so that we find it unnecessary to include any spatial anisotropy of the VB in the computations. For GaAs we use the known effective masses (in units of the free electron mass) of 0.0635 for the CB (at 300 K) and 0.081, 0.643, and 0.172 for the light, heavy, and split-off VBs, and a spin-orbit splitting of 0.341 eV.[34] For the InGaP CB effective mass we use 0.084, with values of 0.137, 0.701, and 0.23 for the light, heavy, and split-off VBs, and a spin-orbit splitting of 0.094 eV.[34] We use dielectric constants of 12.9 and 11.8 for GaAs and InGaP (the latter being an average of the InP and GaP values),[35] respectively, and all of our computations are for a temperature of 300 K.

B. Spectra far from the Heterojunction

To introduce our analysis method we consider spectra acquired sufficiently far from the heterojunction so that the influence of the neighboring layer is negligible. Figure 5 shows a spectrum obtained from a point in the GaAs layer located 4 nm from the junction, and Fig. 6 shows a spectrum acquired from a point in the InGaP layer located 12 nm from the junction. In both figures, experimental spectra are shown by solid lines, and theoretical spectra are shown by the various symbols. All spectra are plotted as conductance at constant tip-sample separation (computed as described at the end of Section II) on a logarithmic scale. The apparent VB onset of the measured spectra in all our experiments is situated far below 0 V, necessitating negative contact potentials with rather large magnitude. (Making the contact potential more negative produces a shift in the computed spectra to more negative voltages, with this shift being some fraction [about 0.3, for the present situation] of the change in contact potential). The tip radius is also quite important in determining the tip-induced band bending, with larger values producing more band bending.

As shown in Fig. 5(b), for GaAs, a contact potential of -1.4 eV together with a tip radius of 30 nm produce a good fit of the computed spectra to the experiment. Tip radii of 10 or 50 nm, with appropriate changes to the contact potential, also produce reasonable fits. The ϕ_0 *vs.* voltage characteristics are similar for all the data sets that produce good fits to the data, as pictured in Fig. 5(a). These results for GaAs are quite insensitive to the VB offset between GaAs and InGaP [although for points closer to the heterointerface this dependence increases, through Eqs. (A10) and (A11)]. For the case of InGaP, Fig. 6, the dependence on VB offset is much greater, with the computed spectra shifting to the left as the offset is increased. Again, we find reasonable fits between experiment and theory for tip radii of 30 – 50 nm, and with appropriate choice of the other parameters. For smaller tip radii near 10 nm, localized states at the CB edge start to appear and contribute to the conductance there, as seen in Fig. 6(b) and discussed in detail in Ref. [6].

The most important parameter in our theory is the contact potential, with values near -1.4 eV found in Figs. 5 and 6 to produce best fits to the data. Our probe tips are composed of Pt-Ir, for which a clean surface is expected to have a work function close to that of bare Pt or Ir of about 5.8 eV.[36,37] But, importantly, a Pt surface which has been oxidized and subsequently heated (as done during our tip preparation) is known to have a significantly lower work function of about 4.6 eV.[38] From the discussion following Eq. (2) this value of tip work function implies a contact potential of about -0.9 eV. This value is somewhat lower in magnitude than the -1.4 eV found from the fits, although we do not consider this discrepancy to be serious since the actual structure of the tip apex is unknown.

In typical STM experiments the tip radii are usually larger than 10 nm,[4] consistent with the values found in Figs. 5 and 6. The opening angle of the tip shank can also be specified in the theory, but we keep this fixed at 90° for all our computations. The results

in Figs. 5 and 6 are for tip-sample separations of 0.9 and 0.8 nm, respectively.[39] Smaller values of tip-sample separation produce larger amounts of band bending, although this dependence is relatively weak for the physically reasonable range of separations, about 0.9 ± 0.2 nm on the basis of prior studies.[4]

An additional parameter in the theory concerns the magnitude of the computed current; in our theory we compute a current density, and multiplying by a tip area produces a current that can be compared with experiment. As discussed in Ref. [6], computations of the type shown in Figs. 5 and 6 for tip-sample separations in the range 0.7 – 0.9 nm lead to deduced tip areas in the range 0.01 – 1 nm^2; these values are physically reasonable, corresponding to current through a single atom or an area of a few atomic-distances on a side.

C. Spectra across the Heterojunction

We now turn to the spectra of Fig. 2, acquired across the InGaP/GaAs heterojunction. This data is shown by the lines in Fig. 7, plotted as conductance at constant tip-sample separation. We generate sets of theoretical spectra and fit those to the experiment. We use a model containing four nonlinear parameters: the tip-sample separation s, the tip radius R, the contact potential between tip and sample $\Delta\phi$, and the VB offset ΔE_V between GaAs and InGaP. In addition, a single amplitude parameter for the entire set of spectra is employed, with the relative amplitudes between spectra determined by the requirement of a constant value (0.1 nA) for the computed current at a sample voltage of -2 V. This constraint is used to determine the relative tip-sample separations for the various computed spectra, with our reported value of s being the separation for spectrum (a) of the series.

Our best fit between experiment and theory is shown in Fig. 7. We find that the theory does indeed provide a good description of the experimental spectra, with the best-fit value for the VB offset being 382 ± 7 meV. We note that the wavefunction tails extending from the GaAs into the InGaP are reasonably well described by the theory (even though the dispersion of these states in the vacuum is neglected, as discussed in the Appendix); the inset of Fig. 7 shows the negative voltage side of spectrum (d), with and without these evanescent states included.

Fitting between experiment and theory is accomplished using a simplex algorithm to search for the minimum in the sum of squared residuals (SSR). The fits are performed using the natural logarithm of the conductance, at the set of 111 voltage values shown in Fig. 7. Values of the SSR are fit to a quadratic form in order to determine the second derivatives, from which error values on the parameters are deduced using the standard methods of least-squares fitting. Specifically, the errors reflect the amount by which a parameter must change, with all other parameters varied optimally, to produce a fractional change in the minimum SSR value of $1/(N-p)$ where $N = 111$ is the number of data points and $p = 5$ is the number of parameters.[40] By this criterion a 1% change in

the SSR is statistically significant in the present case (at a level of one standard deviation), assuming that our theory truly describes the data.

The relative amplitudes of the theoretical spectra in Fig. 7 are determined by the requirement of constant current at the starting point of each spectrum. To further explore the fit between experiment and theory we compare the computed constant-current contour with the experimental one. The observed tip height contour is shown by curve (a) in Fig. 8, taken from a cut of the same data set of Fig. 2(A).[41] The theoretical contour, computed with the parameters of Fig. 7, is shown by Fig. 8(b). A correction to the theory has been included here due to elastic strain effects, as shown by Fig. 8(c) taken from theoretical curve (f) of Fig. 1(B). We find reasonably good agreement between Figs. 8(a) and (b), particularly in terms of the overall tip displacement between the GaAs and InGaP layers. The detailed shape of the transition region between the GaAs and the InGaP is somewhat different between experiment and theory; this could involve additional effects of the elastic deformation of the surface and/or a small amount of tip convolution, neither of which we further investigate here.

D. Additional Parameters

We have investigated the influence on the fits of extrinsic surface states. Parameters are introduced for describing the density and the energy distribution of the states. It is also necessary to specify a particular energy, known as the charge neutrality level, above which the states are charged negative when occupied by an electron and neutral when empty (*i.e.* acceptor states) and below which they are neutral when occupied and positive when empty (*i.e.* donor states). We first consider a model in which the spectrum of extrinsic states is distributed *uniformly* across the band gap, with charge neutrality level at the midgap energy of GaAs (*i.e.* as used in Refs. [4] and [5]). For densities below $0.01\,\mathrm{nm}^{-2}\mathrm{eV}^{-1}$ the fits are slightly worse than in the absence of extrinsic states, and for higher densities the fits become much worse. We have also varied the charge neutrality level throughout the gap, and found no improvement in the resulting fits. We have furthermore considered other models for the energy spectrum of the states, in particular considering a localized distribution of states and moving that distribution through the band gap. Donor-like states were found to give better fits than acceptor-like ones, but again all fits were worse than those in the absence of extrinsic states.

Another possible source of parameter variation in the model concerns the contact potential between the tip and the sample. Thus far we have assumed identical contact potentials for the tip-GaAs and the tip-InGaP junctions. In other words, we have assumed that the vacuum levels of the GaAs and InGaP surfaces are coincident. Their vacuum levels could be slightly different, however, due to either a microscopic interface dipole at the InGaP/GaAs heterojunction[42] or a difference between the surface dipoles of the two materials.[43] For these (110) surfaces the surface dipoles involve the buckling relaxation of the surface;[44] presumably a difference between surface dipoles of III-V (110) surfaces could be computed from first-principles theory, although we are not aware of any such results in the literature. Nevertheless, considering the buckling using effective charges of the surface Ga and As atoms,[45] we estimate that a difference of around 0.1 eV or less

between the surface dipoles is entirely possible. Concerning an interface dipole, first-principles theory indicates that any such dipole at the InGaP/GaAs heterojunction is quite small,[18,19] but in any case distinguishing between an interface dipole or a difference between surface dipoles is not possible in our experiment.

We have investigated fits that include an additional parameter, $\delta\phi$, defined as the tip-InGaP contact potential minus the tip-GaAs contact potential [*i.e.* equal to the vacuum level energy of the InGaP(110) surface relative to that of the GaAs(110) surface]. We find that the best-fit VB offset values are rather sensitive to the value of $\delta\phi$. Essentially, nonzero $\delta\phi$ values produce a *lateral* field across the heterojunction, which then shifts the value of the VB offset. For $\delta\phi$ values near 0.1 eV we find a small improvement in the fit (SSR value of 14.1) for a VB offset value of 362 meV. However, for such fits we also find that the constant-current contours (of the type shown in Fig. 8) change significantly. We define by Δz the height of the contour over the GaAs compared to the InGaP, considering a point located 2 nm into the GaAs layer compared to one located 6 nm into the InGaP layer, and we find that Δz depends sensitively on $\delta\phi$. The experimental Δz value from Fig. 8(a) is 0.095 ± 0.003 nm, which agrees well with the theoretical value (assuming $\delta\phi = 0$) of 0.094 nm from Fig. 8(b). For $\delta\phi = 0.1$ eV (and a VB offset of 362 meV) the theoretical Δz value increases to 0.118 nm, which is far outside the experimental range. Thus, we can further constrain the fits by matching the Δz values between experiment and theory. Using this method, we find that the lateral field across the heterointerface is very close to zero, and the best-fit value for the VB offset is essentially unchanged from the 382 ± 7 meV of Fig. 7. This then is our final result for the VB offset, which we express in round numbers as 0.38 ± 0.01 eV.

V. DISCUSSION

The results of the prior section are for an InGaP-on-GaAs interface. We have also applied our analysis method to the data set of our prior work, Ref. [9], acquired on a GaAs-on-InGaP interface. Those spectra have band edges are shifted to lower (more negative) voltages by about 0.1 V compared to the InGaP-on-GaAs spectra of Fig. 7. Also, several of the spectra in Ref. [9] [spectra (c) and (d) of Fig. 3] display some exceptionally large additional conductance near the CB edge (in the range 1.0 – 1.2 V) compared to the other spectra, indicative of extrinsic states producing local band bending. Indeed, we find that it is impossible to fit those prior spectra without assuming a relatively high density of extrinsic states in the vicinity of spectra (c) and (d). For example, assuming $0.2\ \text{nm}^{-2}$ of donor-like states spread over a circular area of $4\ \text{nm}^2$ (corresponding to about 1 fundamental unit of charge) produces a relatively good fit, with a VB offset of about 370 meV. However, assumptions concerning the magnitude and placement of this charge produce significant uncertainty in this band offset, of at least ± 30 meV. We find, in general, that precise evaluation of the band offset can only be obtained from data sets that display no evidence of spatially inhomogeneous extrinsic states.

Finally, we return to re-examine the analysis method used in our previous work, and also shown in Fig. 2 of the present work, in which we overlaid the normalized conductance spectra acquired in the GaAs and InGaP regions and deduced a very small CB offset (about 0.03 eV in Fig. 2, and 0.00 eV in our previous work[9]). These values are clearly incorrect, indicating a failure of this type of analysis method. The normalized conductance used here is meant to provide a spectral measurement that is roughly independent of tip-sample separation, but importantly, *that independence only occurs if the spectra are measured over a sufficient range ($\approx 1.0\,V$) beyond a band onset*. This limitation in the analysis method was not fully appreciated in our previous work, but it can be deduced by an extension of our subsequent analysis in Ref. [5]. Our spectra acquired on the InGaP/GaAs heterojunctions have a rather limited voltage range; the band bending is quite large at negative voltages [as seen in Fig. 5(a) or Fig. 6(a)], with tunneling through the depletion region in the semiconductor [as in Fig. 4(b)] producing a large effect on the current over the entire voltage range. For this reason, the normalized conductance cannot be used as a reliable means of determining band onsets.

VI. CONCLUSION

In conclusion, scanning tunneling spectroscopy has been used to study the electronic properties of InGaAs-like InGaP/GaAs interfaces. The observed spectra are fit to computational results, assuming an InGaP band gap of 1.90 eV as appropriate for the disordered alloys observed here. We deduce a VB offset of $0.38 \pm 0.01\,\mathrm{eV}$, which, with our assumed value of 1.90 eV for the InGaP band gap and using 1.42 eV for the GaAs gap, yields a value for the CB offset of $0.10 \pm 0.01\,\mathrm{eV}$. These values were obtained from an InGaP-on-GaAs interface. Results for a GaAs-on-InGaP interface are consistent with these values, although much greater uncertainty occurs in that case due to the presence of extrinsic (charged) surface states. Comparing our result to prior measurements of the band offsets,[10-17] we note that some spread exists in those values but our result is near the middle of that range. It is also notable that our values are in fairly good agreement with the theoretical results of Froyen *et al*.[19] of 0.37 and 0.12 eV for the VB and CB, respectively.

Regarding possible extensions to the present work, two approximations that could be improved upon is the neglect of the dispersion across the vacuum gap of the states near the interface, and the neglect of any image potential effects.[46] Beyond that, we note that our use of the effective mass approximation could be replaced by a more sophisticated multi-band complex-$\mathbf{k}$ band structure,[47] as commonly used in semiconductor heterostructure problems. That change would yield an improved description of the spectra for energies far from the band edges. The other major approximation employed in this work is our solution for the tunnel current using a planar approximation, *i.e.* using only the potential along the central axis of the system, an approximation that is equivalent to a semiclassical treatment of the lateral (radial) part of the electronic states. An improved description would require a fully 3D quantum treatment of the electronic states. We note that any of these potential improvements would be quite computationally intensive; the results of the present work required, for a single fit with 4 nonlinear parameters, about 2

months of computation time using a 2.8-GHz processor, and to accomplish all the fits described herein we utilized seven such processors over a period of one year.

Despite the approximations in the theory, we feel that the error range assigned to the band offsets, $\pm 0.01\,\mathrm{eV}$, is realistic. This range was deduced primarily from statistical uncertainty in the fitting procedure. However, we find a similar error range when we have applied the curve fitting procedure with other computational schemes that produce slightly different shapes for the conductance *vs.* voltage curves, *e.g.* with different boundaries conditions for the wavefunctions, as was done during the development of the theory. Such changes in shape can significantly influence the values of parameters such as the tip radius or tip-sample separation, since they are dependent on the detailed shape of the spectra. But the band offset is largely determined by the difference in position of the band edges between spectra acquired on the GaAs and InGaP surfaces, *i.e.* it just produces an offset between these respective spectra, and hence is relatively independent of the theoretical details that affect the shape of the spectra. In other words, so long as a good fit can be obtained to the spectra using some values for tip radius, tip-sample separation, and tip-sample contact potential – and these might be *effective* values, dependent on the approximations in the theory – then extracting a band offset is something that we believe can be reliably achieved even within the approximate theory.

Acknowledgments

This work was supported by the National Science Foundation, grant DMR-0503748, and by the Deutsche Forschungsgemeinschaft. Discussions with M. Hybertsen and A. Zunger are gratefully acknowledged. We also thank R. Duca and S. Gaan for their careful readings and criticism of this manuscript. We are grateful to the Undergraduate Physics Laboratories at Carnegie Mellon University for providing the computer resources used in this work.

Appendix: Tunnel current near a semiconductor heterointerface

For the present problem of computing tunnel currents near an interface between two different semiconductors, our prior theory for a homogeneous semiconductor[3,4,5,6] must be generalized. For the electrostatic potential we remove the previous assumption of circular symmetry and include an explicit dependence on the azimuthal angle θ. We follow in detail the notation and definitions in Ref. [3]. Laplace's equation for the electrostatic potential energy ϕ in the vacuum, using prolate spheroidal coordinates, is given by

$$\frac{\partial}{\partial\xi}\left[\left(\xi^2-1\right)\frac{\partial\phi}{\partial\xi}\right]+\frac{\partial}{\partial\eta}\left[\left(1-\eta^2\right)\frac{\partial\phi}{\partial\eta}\right]+\frac{\xi^2-\eta^2}{(\xi^2-1)(1-\eta^2)}\frac{\partial^2\phi}{\partial\theta^2}=0 \quad . \tag{A1}$$

On a discrete grid of points (ξ_i,η_j,θ_k), i = 1, 2,... m; j = 1, 2,... n; k = 1, 2,... p, we put this equation into finite-difference form according to

$$\begin{aligned}\left[\frac{2(\xi_i^2-1)}{(\Delta\xi_i)^2}+\frac{2(1-\eta_j^2)}{(\Delta\eta_j)^2}+\frac{2(\xi_i^2-\eta_j^2)}{(\xi_i^2-1)(1-\eta_j^2)(\Delta\theta_k)^2}\right]\phi_{ijk}\,=\\ \frac{(\xi_i^2-1)}{(\Delta\xi_i)^2}(\phi_{i+1,j,k}+\phi_{i-1,j,k})+\frac{(1-\eta_j^2)}{(\Delta\eta_j)^2}(\phi_{i,j+1,k}+\phi_{i,j-1,k})\\ +\frac{\xi_i}{\Delta\xi_i}(\phi_{i+1,j,k}-\phi_{i-1,j,k})-\frac{\eta_j}{\Delta\eta_j}(\phi_{i,j+1,k}-\phi_{i,j-1,k})\\ +\frac{(\xi_i^2-\eta_j^2)}{(\xi_i^2-1)(1-\eta_j^2)(\Delta\theta_k)^2}(\phi_{i,j,k+1}+\phi_{i,j,k-1}) \quad .\end{aligned} \tag{A2}$$

We use a uniform grid spacing for η, and we match the ξ values at the surface to the r values in the semiconductor as specified below. For the θ values we use a uniform spacing with $\theta_k=(k-0.5)\Delta\theta$ and $\Delta\theta=2\pi/p$ for a general problem or $\Delta\theta=\pi/p$ for a problem with mirror symmetry on the surface. Potential values are repeated periodically in θ appropriately for either case. To put Eq. (A2) into a form suitable for iterative solution we assign the value of ϕ_{ijk} on the left-hand side to be its value on the $(\ell+1)^{\text{st}}$ iteration, with all the ϕ values on the right-hand side of the equation being those on the ℓ^{th} iteration.

In the semiconductor we use variable grid spacing for *r* and *z*, as defined in Appendix B of Ref. [4], and we use the same θ values as in the vacuum. Poisson's equation in discrete form, using cylindrical coordinates, is rearranged to yield

$$\left[\frac{2}{(\Delta r_i)^2}+\frac{2}{(\Delta z_j)^2}+\frac{2}{r_i^2(\Delta\theta_k)^2}\right]\phi_{ijk}=$$
$$\frac{1}{(\Delta r_i)^2}(\phi_{i+1,j,k}+\phi_{i-1,j,k})+\frac{1}{(\Delta z_j)^2}(\phi_{i,j+1,k}+\phi_{i,j-1,k})$$
$$+\frac{1}{(2r_i\Delta r_i)}(\phi_{i+1,j,k}-\phi_{i-1,j,k})+\frac{1}{r_i^2(\Delta\theta_k)^2}(\phi_{i,j,k+1}+\phi_{i,j,k-1}) \qquad \text{(A3)}$$
$$-\frac{e}{\varepsilon_{ijk}\,\varepsilon_0}\rho_{ijk} \quad .$$

where ρ_{ijk} is the charge density and ε_{ijk} the dielectric constant at each point in the semiconductor. In a semi-classical approximation for a uniform material, the charge density is given by $\rho_{ijk} \equiv \rho(E_F - \phi_{ijk})$ with E_F being the Fermi-level. For the present problem of a heterostructure an additional index, *r*, is required to distinguish between the two materials, $\rho_{ijk} \equiv \rho_r(E_F - \phi_{ijk})$ with *r* taking on an appropriate value depending on which material the spatial point is located in. The dielectric constant is similarly determined, $\varepsilon_{ijk} = \varepsilon_r$. We consider a problem of a slab of material (quantum well or barrier) which we denote by $r = 2$, surrounded on either side by cladding material, denoted by $r = 1$. The Fermi-level for the system is determined by charge neutrality in the cladding material, $\rho_1(E_F) = 0$, with the charge densities determined by the doping and band gap of the material precisely as specified in Ref. [3]. With specification of a valence band offset, $\Delta E_V \equiv E_{V,2} - E_{V,1}$, the band extrema in the slab are then determined relative to E_F, and the charge densities in the slab (as a function of $E_F - \phi_{ijk}$) can be computed. At each iteration of our finite-difference solution, Eq. (A3) is solved for ϕ_{ijk} by using a 1-dimensional search to solve the relevant nonlinear equation, as described in Ref. [3] (see also footnote [36] of Ref. [4]). With differing dielectric constants between the materials, we must also include the condition that the normal component of the electric displacement is continuous across the heterointerface. This condition leads to an additional equation connecting the potential values on either side of the interface, which we solve simultaneously with Eq. (A3).

For reasons of computational efficiency we find it necessary to make one additional modification to the coordinate system in the vacuum, in which we generalize the prolate spheroidal coordinates into a new coordinate system that exactly matches the hyperbolic shape of the probe tip. The tip shape is specified by its radius of curvature *R*, the slope of the tip shank *b*, and the tip-sample separation *s*. The reason that new coordinates are needed is that, within the prolate spheroidal system, only *two* of these tip parameters can be exactly matched to the coordinate system, so that for an arbitrary tip shape it is necessary for the tip itself to fill some of the grid points in the vacuum.[3] As the tip-sample separation changes then the grid points occupied by the tip will change, leading to small discontinuities in the computed potentials. The size of these discontinuities

decreases as the density of grid points increases, but for the large number of finite-difference computations needed in our curve fitting the use of such dense grids is prohibitive. With our new coordinate system these discontinuities in the potential are eliminated. The new coordinates $\tilde{\xi}$ and $\tilde{\eta}$ in the vacuum are related to the cylindrical coordinates r and z by

$$\frac{r^2}{\tilde{\xi}^2 - 1} + \frac{(z - ac\tilde{\eta})^2}{\tilde{\xi}^2} = a^2, \tag{A4a}$$

$$-\frac{r^2}{1 - \tilde{\eta}^2} + \frac{(z - ac\tilde{\eta})^2}{\tilde{\eta}^2} = a^2 \tag{A4b}$$

where $c \equiv z_0 / (a\tilde{\eta}_T)$ with $\tilde{\eta}_T$ being the $\tilde{\eta}$ value defining the hyperbola that corresponds to the boundary of the probe tip and z_0 being the center point of this hyperbola. For $z_0 = 0$ these equations reduce to the standard definition of prolate spheroidal coordinates. With specified values for R, b, and s we have $\tilde{\eta}_T = 1/\sqrt{1 + b^2}$, $a = Rb^2 / \tilde{\eta}_T$, and $z_0 = s - a\tilde{\eta}_T$. From Eqs. (A4a) and (A4b), Laplace's equation in the new coordinates can be deduced in a straightforward, though lengthy, manner. This equation is then cast into finite-difference form in a manner analogous to Eq. (A2).

With the electrostatic potential determined in the above manner, tunnel currents are computed in the effective mass approximation by adding this potential onto the vacuum level or onto the relevant band edge energy in the tip or semiconductor. We extend our previous theory for a homogeneous semiconductor[6] to handle a heterojunction. We maintain the *z*-coordinate to be perpendicular to the surface and we take *x*-coordinate to be perpendicular to the junction. For definiteness we consider a type-I junction, with VB and CB edges of the smaller-gap quantum well located within the band gap of the larger-gap barrier layer, although the formalism below can be easily modified for other situations. For computation of the tunnel current we maintain our planar approximation, so we do not consider any lateral variation in the potential in computing the current. In this case, we need only consider the wavefunction tails, or *evanescent states*, extending into the barrier from the quantum well. We make a further approximation for this situation, assuming that the effective masses in the barrier and well are identical, so that any given state in the barrier (well) is analytically connected to a *single* state in the well (barrier) without having to consider linear combinations of such states.

To handle a situation of spatially resolved STS across a heterojunction we must modify our prior expressions for the tunnel current, Eqs. (9) and (11) of Ref. [6], so that they explicitly contains some dependence on the lateral, (*x,y*), position of the probe tip. It is also convenient, though not essential, to also remove as much as possible from these equations their dependence on the tip electronic states. Following in detail the notation and definitions of Ref. [6] we consider a probe tip with a very low-lying minimum energy of its metallic band, $E_0 \to -\infty$, so that $k_{\perp,\mathrm{R}} \to k_F$ the Fermi-wavevector of the metallic band. The matrix element for the tunnel current is evaluated at a position z_1 at the surface of the probe tip; both the tip and sample wavefunctions decay exponentially into

the vacuum with decay constant $\kappa = \{2m[U(s) - E_\perp]/\hbar^2\}^{1/2}$ using the potential energy in the vacuum from Eq. (4) of Ref. [6], so that their derivatives can be evaluated as simply $\pm\kappa$ times the wavefunction value. All dependence on the tip wavefunctions other than a factor of k_F is thereby eliminated from the formulas, and we find that the tunnel current for a homogeneous semiconductor can be written in the form

$$J = \frac{2e}{h}\int_{-\infty}^{\infty} dE\,[f(E) - f(E - eV)]\int_0^{\infty} k_{||}\,dk_{||}\,\frac{4\hbar^2\kappa^2}{mk_F}N_\perp(E_\perp)\left|\psi_{k_\perp}(s)\right|^2 \quad \text{(A5)}$$

where $\psi_{k_\perp}(s)$ is perpendicular part of the sample wavefunction evaluated at the tip surface, and where the perpendicular density of states is given for extended (writing the result for a CB) or localized states by

$$N_\perp(E_\perp) = \begin{cases} \dfrac{m^* L}{\pi\hbar^2 k_\perp}\,\theta(E_\perp - E_C) & \text{extended} \\ \displaystyle\sum_\mu \delta(E_\perp - E_\mu) & \text{localized} \end{cases} \quad \text{(A6)}$$

with L being a normalization length in the perpendicular direction and where the formulas for $k_\perp$ and $E_\perp$ are given following Eq. (7) of Ref. [6] (the appropriate formulas for a VB are also given there). For the situations of interest described in the present work we have numerically tested the above approximation of $E_0 \to -\infty$ compared to a typical value of E_0 being 8 eV below the tip Fermi-level, and we find it leads to only a few percent error in the voltage-dependence of the current.

To include in our equations an explicit dependence on lateral position from the heterointerface, we first make the trivial substitution for the integral over $k_{||}$,

$$\int_0^{\infty} k_{||}\,dk_{||} = \frac{1}{2\pi}\int_{-\infty}^{\infty} dk_x \int_{-\infty}^{\infty} dk_y\,. \quad \text{(A7)}$$

Next we rework the derivation of Eq. (A5), but using the approximation of Tersoff and Hamann for a sharp tip.[33] Considering the matrix element for the tunneling process, Eq. (6) of Ref. [6], in the derivation by Duke[48] for a planar geometry this surface integral reduces to simply integrating the plane waves that form the parallel parts the tip and sample wavefunction, hence leading to the δ-function in $\mathbf{k}_{||}$. However, considering a very sharp tip, this surface integral yields the parallel part of the sample wavefunction evaluated at the position of the tip, times a factor of $\sqrt{A}$ where A is a normalization area. Thus, in this approximation, the result for the current density obtained with a sharp tip can be obtained from Eq. (A5) by the substitution

$$\left|\psi_{k_\perp}(s)\right|^2 \to A\left|\Psi_{k_x k_y k_\perp}(x, y, s)\right|^2 \quad \text{(A8)}$$

where $\Psi_{k_x k_y k_\perp}(x,y,s)$ is the total wavefunction of the sample evaluated at the position of the tip apex.

We write the total wavefunction as

$$\Psi_{k_x k_y k_\perp}(x,y,s) = \chi_{k_x}(x)\frac{1}{\sqrt{\ell}}e^{ik_y y}\psi_{k_\perp}(s) \tag{A9}$$

with $\ell = \sqrt{A}$ being a normalization length. This equation defines the *x*-component of the wavefunction $\chi_{k_x}(x)$. In assuming this separable form we are neglecting the dispersion (*i.e.* change in shape) of the *x*-component of the wavefunction across the vacuum gap, which is expected to be relatively small for the 1-nm-wide gap. Thus, the problem has been reduced to the well-known situation of scattering over or tunneling into a barrier.[49] We consider for definiteness a CB barrier of ΔE_C extending over $x > 0$. For an *x*-component of the energy below the barrier the states have the form

$$\left|\chi_{k_x}(x)\right|^2 = \begin{cases} \frac{2}{\ell}\cos^2\left(k_x x - \frac{\alpha}{2}\right) & x < 0 \quad \text{(A10a)} \\ \frac{2}{\ell}\cos^2\left(\frac{\alpha}{2}\right)e^{-2\beta x} & x \geq 0 \quad \text{(A10b)} \end{cases}$$

where $\beta = [(2m^*\Delta E_C/\hbar^2) - k_x^2]^{1/2}$ and $\alpha = -2\cos^{-1}[k_x/(k_x^2+\beta^2)^{1/2}]$. For an *x*-component of the energy above the barrier we construct standing wave solutions for a barrier layer with thickness *d* in the center of a slab of thickness ℓ. We consider solutions for $\ell \to \infty$ and for large values of *d*, in which case we find that[50]

$$\left|\chi_{k_x}(x)\right|^2 = \begin{cases} \frac{1}{\ell}\left[1 + r\cos(2k_x x)\right] & x < 0 \quad \text{(A11a)} \\ \frac{k_x}{\ell k_x'}\left[1 - r\cos(2k_x' x)\right] & x \geq 0 \quad \text{(A11b)} \end{cases}$$

where $r = (k_x - k_x')/(k_x + k_x')$ with $k_x' = [k_x^2 - (2m^*\Delta E_C/\hbar^2)]^{1/2}$ being the *x*-component of the wavevector in the barrier layer. Results for the VB can be obtained simply by substituting ΔE_V for ΔE_C. Using Eqs. (A6) – (A11) in Eq. (A5) enables computation of the tunnel current at any point relative to the heterointerface.

The above theory is valid for identical effective masses across the heterointerface, although for the actual problem the masses for the quantum well and barrier material are different. In our computations for extended states, for a tip location above a given material, we use the effective masses appropriate to that material. The change in computed tunnel spectra as we move across the heterointerface is relatively small, *i.e.* smaller than the deviation between experimental and theoretical spectra for either tip position, so that this procedure seems reasonable. For the case of evanescent states in the barrier we have the choice between using the effective masses of the well material (which determine the number of states) or the barrier (which determines the decay of the states); numerically the difference between these two situations is not large, and we use the former method here.

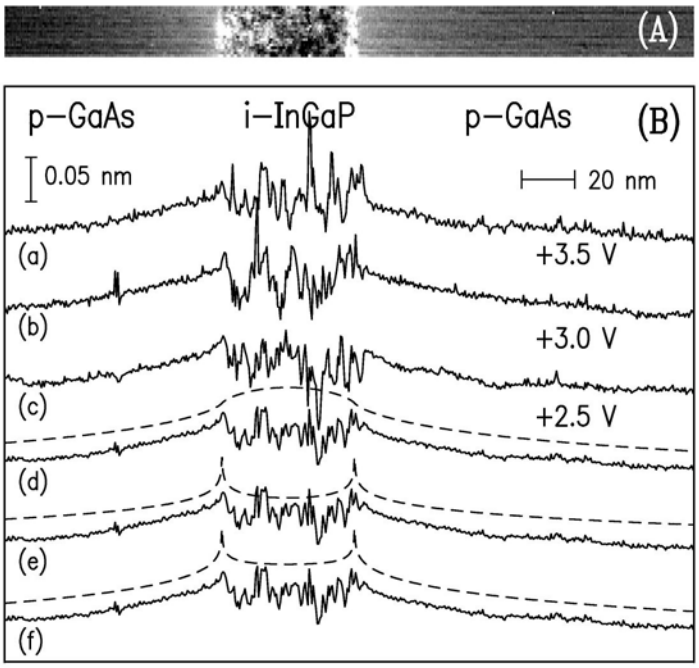

FIG 1. (A) STM image of the heterostructure at sample voltage of $+2.5$ V . The image is displayed with a gray scale of 0.11 nm. (B) (a) – (c) STM topography line scans, acquired at the sample voltages indicated. (d) – (f) Solid lines show the average of the experimental curves from (a) – (c), respectively. Dashed lines show theoretical predictions, assuming (d) 0.06% compressive strain only in the InGaP layer, (e) strain only at InGaAs-like interfaces with a single bilayer of 3.36% compressive strain, and (f) strain both in the InGaP layer (0.02% compressive) and at InGaAs-like interfaces [same condition as curve (e)].

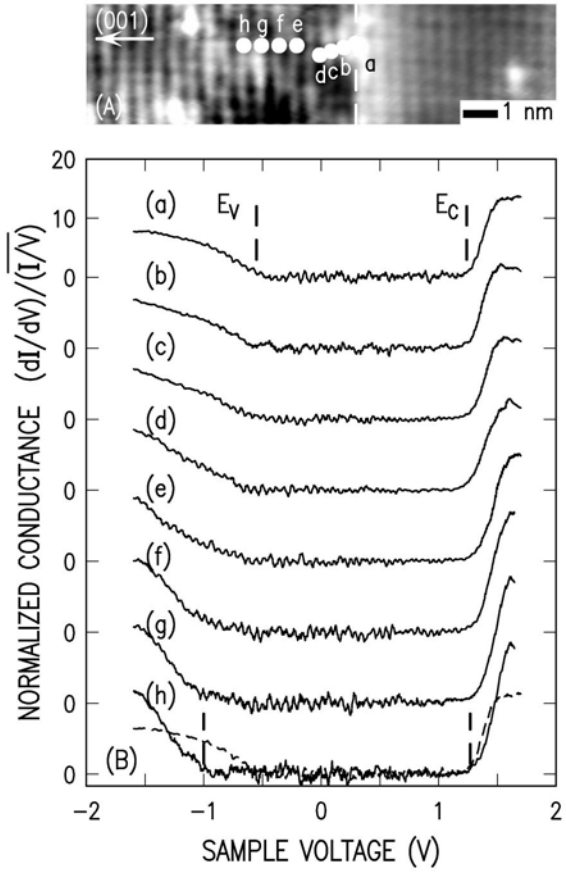

FIG 2. (A) Atomic resolution STM image of InGaP-on-GaAs interface. The image was acquired with sample voltage of –2.0 V and is displayed with a gray scale of 0.05 nm. White circles represent positions where spectra are taken. The dashed line in the image labels the interface, with the InGaP layer being on the left side of the interface and the GaAs layer on the right. (B) Tunneling spectra across the interface. For comparison purposes, spectrum (a) is overlaid as a dashed line on spectrum (h).

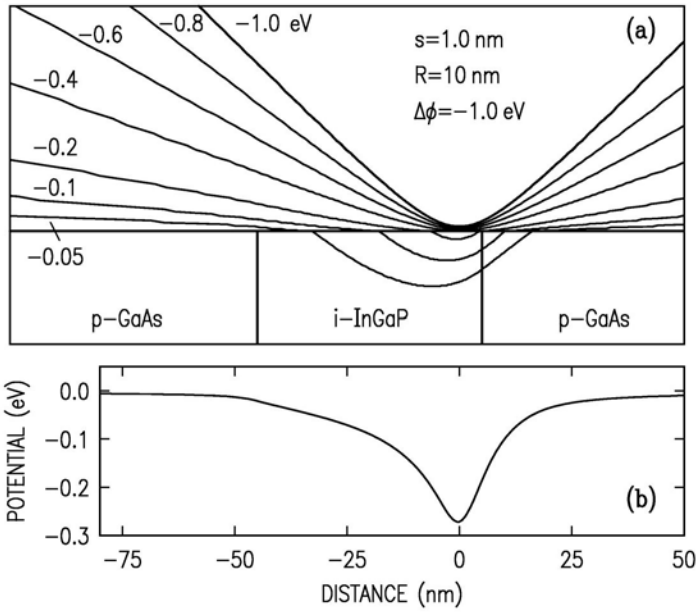

FIG 3. Example of a potential distribution obtained from the theoretical computations, for a tip-sample separation of 1 nm, tip radius of 10 nm, and tip position 1 nm inside the InGaP layer. The tip potential energy is $-1\,\mathrm{eV}$ relative to a point far inside the semiconductor (achieved in this case with a contact potential of $-1\,\mathrm{eV}$ between tip and sample and zero applied voltage between them). Contours of constant potential energy, as labeled, are shown in (a). The variation in the potential energy along the surface is shown in (b).

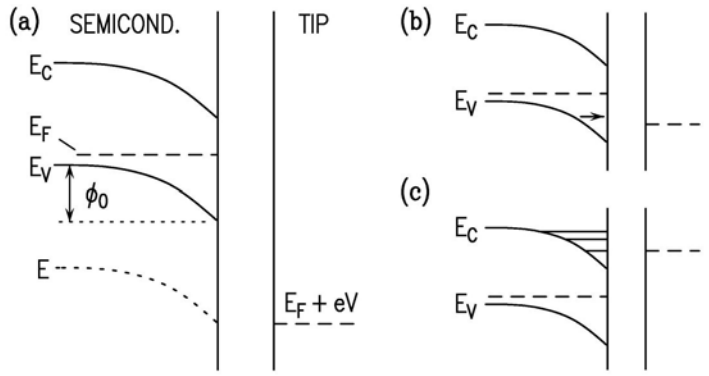

FIG 4. (a) Semiclassical variation (band bending) of energy levels in a semiconductor dues to a varying electrostatic potential, showing the VB maximum at E_V, the CB minimum at E_C, and some representative state at energy E. The sample Fermi-level is denoted by E_F with the tip Fermi-level at $E_F + eV$ where V is the sample voltage. The band bending at the surface is denoted by ϕ_0, with V and ϕ_0 both being negative in this diagram. Quantum effects within the semiconductor are illustrated in (b) and (c) for wavefunction tailing through a depletion region and for localized state formation, respectively.

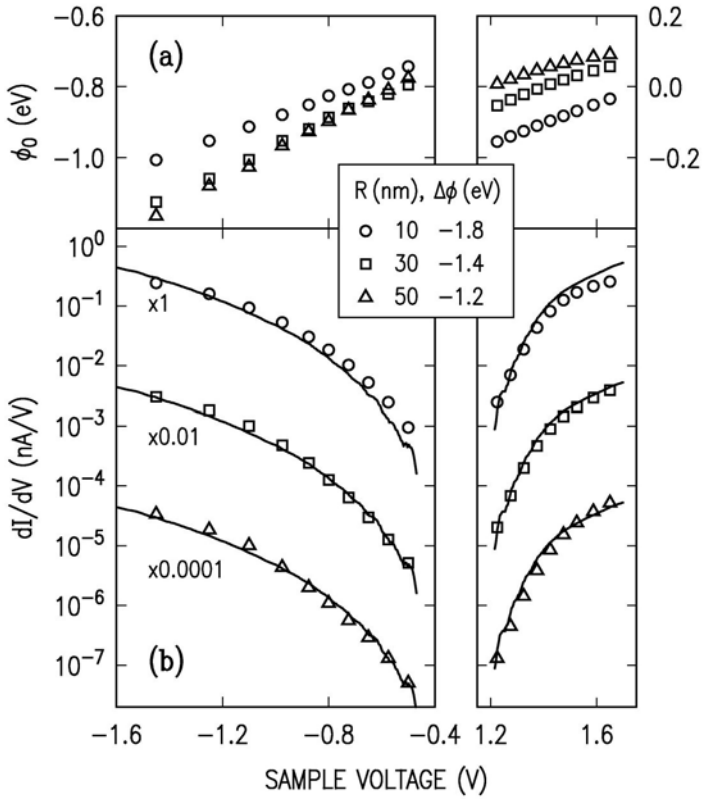

FIG 5. Comparison of theory and experiment for tunneling spectra acquired at a point in the GaAs located 4 nm from the heterointerface. (a) Computed band bending as a function of sample voltage, for various parameters sets. (b) Computed conductance (symbols), compared with a measured spectrum (solid line). The same experimental curve is shown three times, and compared with various theoretical curves for different values of tip radius-of-curvature R and contact potential $\Delta\phi$, as listed. A tip-sample spacing of 0.9 nm is used, together with a VB offset of 0.35 eV.

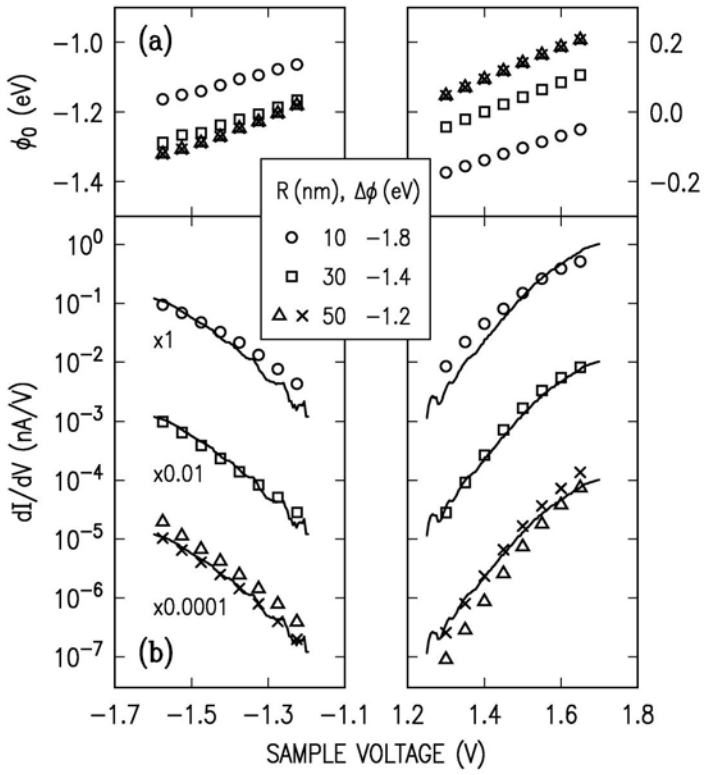

FIG 6. Comparison of theory and experiment for tunneling spectra acquired at a point in the InGaP located 12 nm from the heterointerface. (a) Computed band bending as a function of sample voltage, for various parameters sets. (b) Computed conductance (symbols), compared with a measured spectrum (solid line). The same experimental curve is shown three times, and compared with various theoretical curves for different values of tip radius-of-curvature R and contact potential $\Delta\phi$, as listed. A tip-sample spacing of 0.8 nm is used, together with a VB offset of 0.35 eV except for the theory shown by ×-marks that has a VB offset of 0.38 eV.

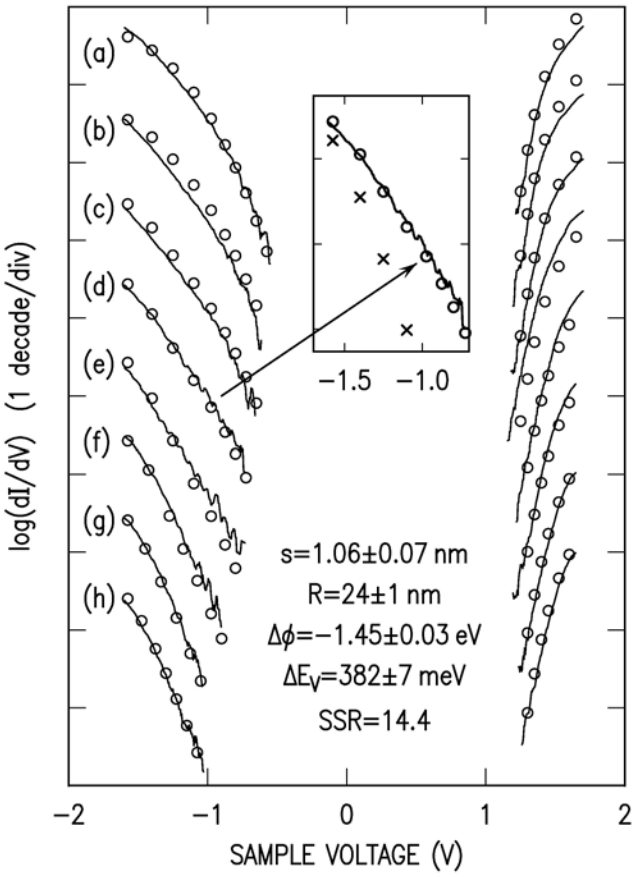

FIG 7. Tunneling spectra acquired across an InGaP-on-GaAs interface, showing the same data as Fig. 2 but plotted as conductance at constant tip-sample separation. Experiment is shown by solid lines and theory by circles. Consecutive pairs of experimental and theoretical curves are displaced by an order-of-magnitude, for ease of viewing. Parameter values for the theory are listed, with s being the tip-sample separation, R the tip radius, $\Delta\phi$ the tip-sample contact potential, and ΔE_V the VB offset. A single amplitude parameter is used for the entire set of spectra. The inset shows the negative voltage side of spectrum (d), with the ×-marks showing a theoretical result in which the current from evanescent states is neglected.

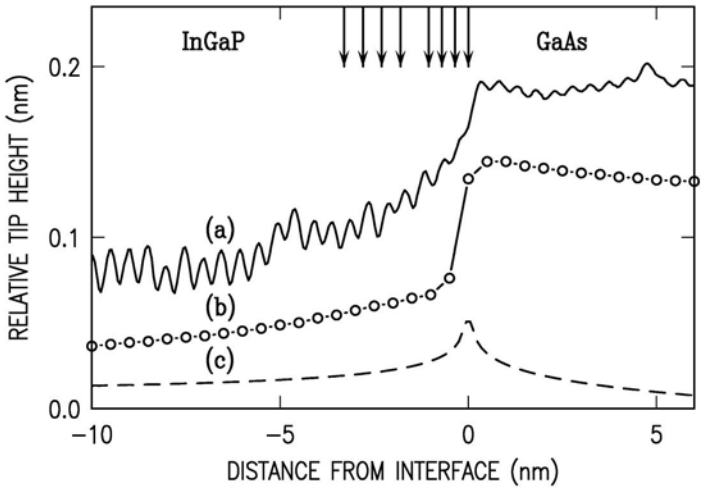

FIG 8. (a) Measured constant-current contour across the InGaP-on-GaAs interface pictured in Fig. 2(A). (b) Computed constant-current contour across the heterointerface, for the parameters listed in Fig. 7. (c) Computed elastic strain of the surface, from curve (f) of Fig. 1(B). The zero of tip height for each curve is arbitrary (some curves have been shifted in height, for ease of viewing). The arrows at the top of the plot indicate the locations at which the spectra of Figs. 2 and 7 were measured.

References:

[1] A. Franciosi and C. G. Van de Walle, Surf. Sci. Rep. **25**, 1 (1996).
[2] H. W. M. Salemink, O. Albrektsen, and P. Koenraad, Phys. Rev. B **45**, 6946 (1992).
[3] R. M. Feenstra, J. Vac. Sci. Technol. B **21**, 2080 (2003).
[4] R. M. Feenstra, S. Gaan, G. Meyer, K. H. Rieder, Phys. Rev. B **71**, 125316 (2005).
[5] R. M. Feenstra, J. Y. Lee, M. H. Kang, G. Meyer, and K. H. Rieder, Phys. Rev. B **73**, 035310 (2006).
[6] R. M. Feenstra, Y. Dong, M. P. Semtsiv, and W. T. Masselink, Nanotechnology **18**, 044015 (2007).
[7] H. Kroemer, J. Vac. Sci. Technol. B **1**, 126 (1983).
[8] C. Nozaki, Y. Ohba, H. Sugawara, S. Yasuami, and T. Nakanisi, J. Cryst. Growth **93**, 406 (1988).
[9] Y. Dong, R. M. Feenstra, M. P. Semtsiv, and W. T. Masselink, Appl. Phys. Lett. **84,** 227 (2004). This paper incorrectly states the growth step immediately following the GaAs layer; it should be a 60 s *exposure* of As, rather than a 60 s "purge" of As.
[10] W. T. Masselink, M. Zachau, T. W. Hickmott, and K. Hendrickson, J. Vac. Sci. Technol. B **10**, 966 (1992); M. Zachau and W. T. Masselink, Appl. Phys. Lett. **60**, 2098 (1992).
[11] M. O. Watanabe, and Y. Ohba, Appl. Phys. Lett. **50**, 906 (1987).
[12] J. H. Chen, J. R. Sites, I. L. Spain, M. J. Hafich, and G. Y. Robinson, Appl. Phys. Lett. **58**, 744 (1991).
[13] T. W. Lee, P. A. Houston, R. Kumar, X. F. Yang, G. Hill, M. Hopkinson, and P. A. Claxton, Appl. Phys. Lett. **60**, 474 (1992).
[14] C. Cai, M. I. Nathan, and T. H. Lim, Appl. Phys. Lett. **74**, 720 (1999).
[15] T. Kobayashi, K. Taira, F. Nakamura, and H. Kawai, J. Appl. Phys. **65**, 4898 (1989).
[16] C. Jelen, S. Slivken, J. Hoff, M. Razeghi, and G. J. Brown, Appl. Phys. Lett. **70**, 360 (1997).
[17] M. A. Haase, M. J. Hafich, and G. Y. Robinson, Appl. Phys. Lett. **58**, 616 (1991).
[18] M. Hybertsen, Mat. Sci. Eng. B **14**, 254 (1992); and private communication.
[19] S. Froyen, A. Zunger, and A. Mascarenhas, Appl. Phys. Lett. **68**, 2852 (1996); A. Zunger, private communication.
[20] N. Liu, C. K. Shih, J. Geisz, A. Mascarenhas, and J. M. Olson, Appl. Phys. Lett. **73**, 1979 (1998).
[21] J. J. O'Shea, C. M. Reaves, S. P. DenBaars, M. A. Chin, and V. Narayanamurti, Appl. Phys. Lett. **69**, 3022 (1996).
[22] R. M. Feenstra, Phys. Rev. B **50**, 4561 (1994).
[23] H. Chen, R. M. Feenstra, P. G. piva, R. D. Goldberg, I. V. Mitchell, G. C. Aers, P. J. Poole, and S. Charbonneau, Appl. Phys. Lett. **75**, 79 (1999).
[24] In contrast, we have also considered band bending effects as a possible source of the gradual drop in the constant-current contour as one moves into the GaAs layer. In that case however the spatial extent of the effect would be limited to only about 20 nm from the heterointerface, *i.e.* a depletion width for a few tenths of an eV band bending. The absence of band bending far from the heterointerface was confirmed by detailed spatially resolved spectroscopy performed in the GaAs that revealed *constant* band

edge positions, within 0.1 V, for distances greater than about 10 nm from the heterointerfaces.

[25] J. H. Davies, D. M. Bruls, J. W. A. M. Vugs, and P. M. Koenraad, J. Appl. Phys. **91**, 4171 (2002).

[26] R. M. Feenstra, Physica B **273-274**, 796 (1999).

[27] N. D. Jäger, M. Marso, M. Salmeron, E. R. Weber, K. Urban, and Ph. Ebert, Phys. Rev. B **67**, 165307 (2003).

[28] In the presence of extrinsic states, the quantity $\Delta\phi$ defined in this work differs from the contact potential measured experimentally since the latter contains an additional term of the band bending due to those states.

[29] J. van Laar, A. Huijser, and T. L. van Rooy, J. Vac. Sci. Technol. **14**, 894 (1977).

[30] For a given energy $E_\perp$ of a state (extended or localized) in the *z*-direction, the wavefunctions in the radial direction in a semiclassical approximation have the form $\exp\left(i\mathbf{k}_{||}\bullet\mathbf{r}\right)$ in classically allowed regions and zero in forbidden regions, with $k_{||}=\left[2m^*\left|E-E_\perp-\phi(x,y,z)\right|/\hbar^2\right]^{1/2}$ at each point in the semiconductor. No tailing of the wavefunction between GaAs and InGaP thus occurs in this approximation.

[31] R. Dombrowski, Chr. Steinebach, Chr. Wittneven, M. Morgenstern, and R. Wiesendanger, Phys. Rev. B **59**, 8043 (1999).

[32] J. Bardeen, Phys. Rev. Lett. **6**, 57 (1961).

[33] J. Tersoff and D. Hamann, Phys. Rev. B 31, 805 (1985).

[34] I. Vurgaftman, J. R. Meyer, L. R. Ram-Mohan, J. Appl. Phys. **89**, 5815 (2001). There is a typographical error in Table IV – the γ_3 value should be 1.25, as stated in the text preceding the table.

[35] *Semiconductors: group IV elements and III-V compounds*, ed. O. Madelung, (Springer-Verlag, Berlin, 1991).

[36] K. M. Tracy, P. J. Hartlieb, S. Einfeldt, R. F. Davis, E. H. Hurt, and R. J. Namenich, J. Appl. Phys. **94**, 3939 (2003).

[37] K. I. Hashim and J. P. Jones, Thin Solid Films **245**, 64 (1994).

[38] J. Lauterbach, K. Asakura, and H. H. Rotermund, Surf. Sci. **313**, 52 (1994).

[39] Specified values of the separation refer to, in all cases, the value at the setpoint (constant current of 0.1 nA, at a sample voltage of -2 V relative to the tip). As detailed in Section II, the separation varies during the spectral measurement according to $s=s_0+a|V|$ where *V* is the sample voltage. The values of a are precisely known for each spectrum, and this same s-variation is used in the computations.

[40] P. R. Bevington and D. K. Robinson, *Data Reduction and Error Analysis for the Physical Sciences*, 3rd ed. (McGraw Hill, New York, 2003), p. 146.

[41] For the STM image of Fig. 2(A) a high-order polynomial has been used as a background subtraction, to permit ease of viewing of the data in the gray-scale format, whereas for Fig. 8(a) this background subtraction is not performed.

[42] A. Franciosi and C. G. Van de Walle, Surf. Sci. Rep. **25**, 1 (1996).

[43] See, *e.g.*, W. R. L. Lambrecht and B. Segall, Phys. Rev. B **41**, 2832 (1990) for some discussion concerning the presence of surface dipoles. Even if no interface dipole

exists at the InGaP/GaAs (001) heterojunction, so that their band offsets are determined by alignment of some common reference level, then slightly differing surface dipoles could still exist at their (110) surfaces.

[44] See, *e.g.*, J. L. A. Alves, J. Hebenstreit, and M. Scheffler, Phys. Rev. B **44**, 6188 (1991).

[45] S. E. Toet and D. Lenstra, Appl. Phys. A **43**, 85 (1987).

[46] G. Binnig, N. Garćia, H. Rohrer, J. M. Soler, and F. Flores, Phys. Rev. B **30**, 4816 (1984); J. Bono and R. H. Good, Surf. Sci. **175**, 415 (1986); Z.-H. Huang, M. Weimer, and R. E. Allen, Phys. Rev. B **48**, 15068 (1993).

[47] See, *e.g.*, Y.-C. Chang, Phys. Rev. B **25**, 605 (1982); D. Z.-Y. Ting, E. Yu, T. C. McGill, Phys. Rev. B **45**, 3583 (1992).

[48] C. B. Duke, *Tunneling in Solids* (Academic Press, New York, 1969), p. 219.

[49] E. Merzbacher, *Quantum Mechanics*, 2nd ed. (Wiley, New York, 1970), p. 88-92.

[50] States with even or odd symmetry relative to the center of the slab are constructed, with periodic boundary conditions across the slab. For $\ell \to \infty$ each of these types of states have spacing in the wavevector $k_x \geq 0$ of $2\pi / \ell$. The results of Eqs. (A10) and (A11) are valid for both even and odd parity states.